eJSE International

Electronic Journal of Structural Engineering 17(2017)

Reinforced Concrete Beams and Slabs with Bonded CFRP Laminates: Strain Compatibility Paradox

E.Y. Sayed-Ahmed*
Professor, Construction Engineering Dept., the American University in Cairo, Egypt
eysahmed@aucegypt.edu

A. A. Abdelrahman
Professor and Head, Structural Engineering Dept., Cairo University, Cairo, Egypt.
aarahman@gega.net

N. G. Shrive
Civil Engineering Dept., the University of Calgary, Canada
ngshrive@ucalgary.ca

ABSTRACT: Externally bonded Fibre Reinforced Polymers (FRP) Laminates have been extensively used to strengthen reinforced concrete beams and slabs in flexure. Most design codes of practice provisions assume full strain compatibility between the FRP laminates and the concrete section in order to estimate the moment resistance of this hybrid system. However, as shown here, strain compatibility is lost during the early stages of loading. The current design methodologies account for premature failure due to interfacial crack debonding mechanisms by limiting the strains in the FRP to low values, resulting in the use of only a small portion of the FRP laminate capacity. Experimental investigations previously performed on precast bridge girders, hollow core slabs, and beam specimens – all with CFRP laminates bonded to their soffits – highlight the loss of strain compatibility and interfacial debonding. In this paper, recommendations are presented in order to tackle both issues.

1 INTRODUCTION

The use of Fibre Reinforced Polymers (FRP) laminates in structural engineering has progressed beyond the experimental stage to implementation in a number of construction projects worldwide. Flexural strengthening of reinforced concrete beams/slabs is one of the major applications, and is commonly performed by bonding FRP laminates to the soffit of the beam/slab. In such cases, failure modes can be separated into two categories based on the duration of composite action between the two materials (Fig. 1). When composite action is maintained until the ultimate load is reached, failure occurs in one of three failure modes depending on the reinforcement ratio and the shear strength of the beam: concrete crushing prior to or following yielding of the steel reinforcement, tensile rupture of the FRP laminates, or shear failure of the concrete beam.

When composite action is not maintained up to the ultimate load, premature failure occurs due to debonding of the FRP laminates from the beam/slab. This failure mode is termed interfacial debonding (Teng et al. 2002, Lu et al., 2005, Sayed-Ahmed et al. 2004 and 2009, Hosny et al. 2006, Bakay et al. 2009, Zhu et al. 2016, Hensher 2016). It is the most common failure mode for beams/slabs strengthened in flexure using externally bonded FRP laminates. Interfacial debonding (Teng et al. 2002, Lu et al., 2005, Smith and Teng 2002a and 2002b, Oehlers wt al. 2003, Teng ta al. 2004, Ombres 2010) may occur due to concrete cover separation along the end of the bonded FRP plate, plate-end interfacial debonding, intermediate (flexure or flexure shear) crack-induced interfacial debonding (IC), or critical diagonal crack-induced interfacial debonding (CDC).

Much of the success of externally FRP-bonded reinforced concrete members strengthening lies in the integrity of the bond between the two materials. The degree to which strain can be transferred, or conversely how much slip occurs in the adhesive, will determine the forces in each material and the overall resistance of the section.

For steel-reinforced concrete, perfect bond is assumed between the concrete and the steel reinforcement. Strain compatibility follows this assumption and, thus, lies at the heart of many analysis and design methods for reinforced concrete. Strain compatibility through the depth of a reinforced concrete section with externally bonded FRP also relies on perfect bond: some experimental investigations support the assumption (e.g. Spadea et al. 1998, Meier 1995, Lee

et al. 1999, Triantafillou and Plevris 1992, Ombres 2012, Choi et al. 2013, Zhou 2013, Hosseini and Mostofinejad 2014, D'Antino 2015).

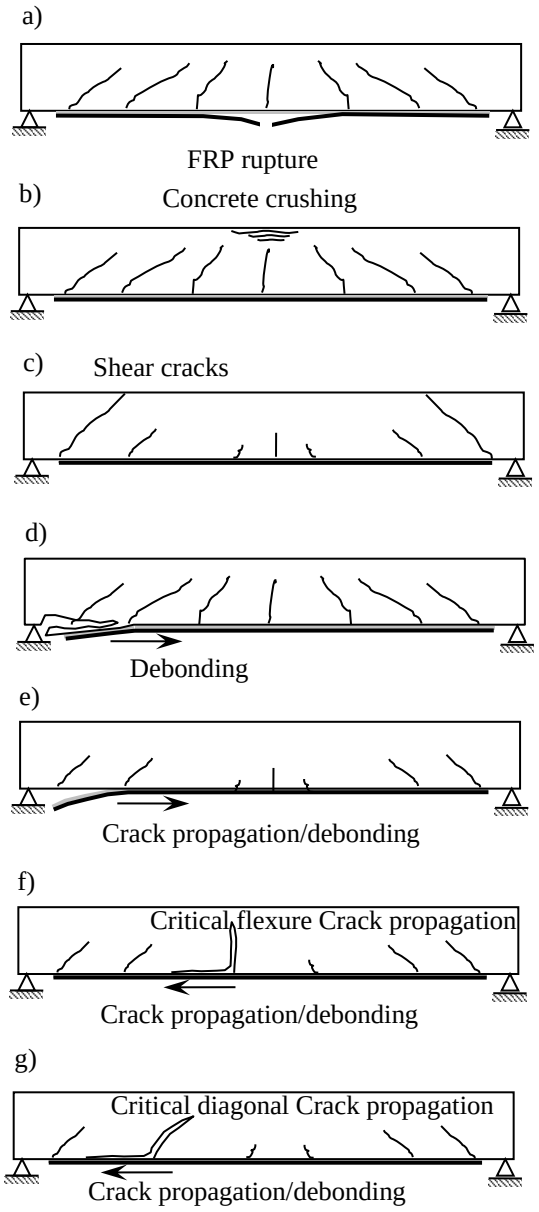

Fig. 1. Failure modes of RC beams with bonded FRP-strips: a) flexure failure by FRP rupture; b) flexure failure by concrete crushing; c) shear failure; d) concrete cover separation; e) plate-end interfacial debonding; f) flexure crack-induced interfacial debonding; g) critical diagonal crack-induced interfacial debonding.

The major factors affecting the bond-slip behaviour (and thus composite action) between the concrete surface and the FRP laminates are the concrete compressive strength, the bond length up to a certain effective length, the axial stiffness of the FRP laminates, the FRP-to-concrete width ratio, the adhesive axial stiffness and the adhesive compressive strength (Lu et al. 2005, Chen and Teng 2001, Uedat et al. 2003, Yuan et al. 2004). Many models have been proposed for describing and determining the bond strength between the FRP laminates and the concrete: these are summarized elsewhere (Sayed-Ahmed et al. 2009). However, further investigations are still needed to reach an effective model for predicting failure due to intermediate crack induced interfacial debonding.

In the current design codes of practice, the calculation of the moment resistance of members with bonded FRP laminates is based on strain compatibility, equilibrium of forces and controlling the mode of failure. However, perfect bond between the FRP laminates and concrete does not always occur. The work presented here is based on three experimental investigations performed by the authors (Sayed-Ahmed et al. 2004, Hosny et al. 2006, Bakay et al. 2009). These investigations involved flexural strengthening with externally bonded FRP to reinforced concrete precast bridge girders, prestressed precast hollow core slabs, and reinforced concrete beam specimens. Premature failure was consistently encountered in all these cases due to interfacial debonding. Strain distributions were recorded during the loading history in the tests, which clearly revealed the lack of strain compatibility. The incompatibility of strains and the premature debonding failures are discussed, and recommendations are outlined tackling the strain limits defined by the ACI 440.2R-08.

2 THE EXPERIMENTAL INVESTIGATION

Three experimental investigations have been performed on: (1) precast reinforced concrete bridge girders strengthened in flexure with soffit-bonded CFRP strips, (2) precast prestressed hollow core slabs strengthened in flexure to resist negative moments using externally bonded CFRP strips to their top surfaces, and (3) reinforced concrete beam specimens tested in the lab with soffit bonded CFRP strips.

2.1 *Precast Reinforced Concrete Bridge Girders Load Combinations*

HC-Type precast girders (Fig. 2) have an inverted U cross-section and are placed, simply supported, beside each other to form the base of the bridge deck. The girders tested were 11.6 m long. Over their service years, these girders had developed major problems. The initial concrete cover provided was too small in comparison to the amount of steel reinforcement; the cover is also deemed to be inadequate based on the current design code. As a result, cracks appeared around the reinforcement, exposing most of the steel in the mid-spans of the girders, with rust developing in the steel bars (Fig. 2).

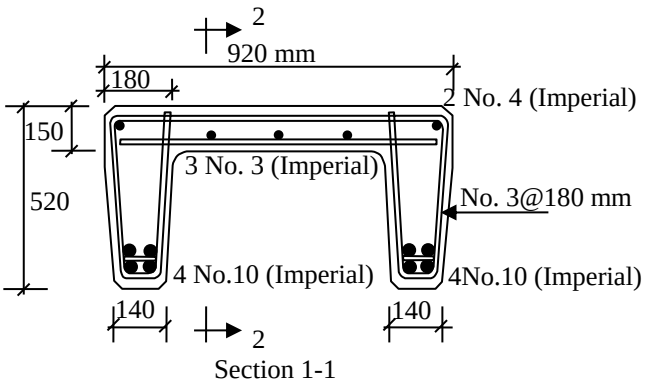

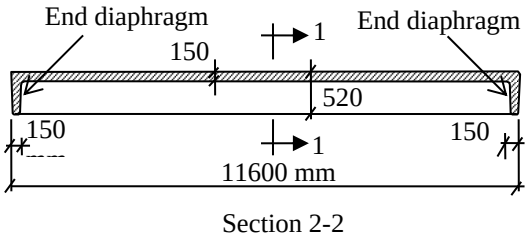

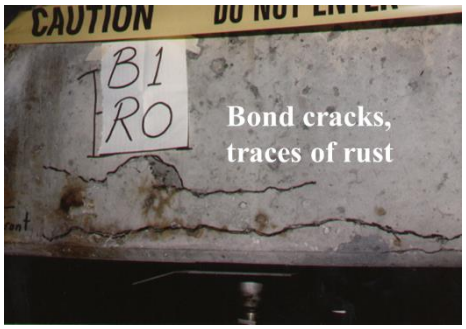

Fig. 2. Cross section and section elevation of an HC-Type precast bridge girder (above) and current girders state (below).

Two girders were patched, strengthened with CarboDur® S1012 CFRP strips (1.2 mm thick × 100 mm width) and Replark® CFRP-sheets (0.12 mm thick × 250 mm width) and tested in flexure using a 4-point load scheme (Fig. 3). The CFRP strips are used to strengthen the girders in flexure while the sheets are used to increase its shear strength and anchor the strips at their ends. The modulus of elasticity, the tensile strength and the maximum elongation of the CFRP strips are 165 GPa, 3050 GPa and 1.7, respectively; while those for the CFRP sheets are 230 GPa, 3400 GPa and 1.55%, respectively.

Strain gauges were mounted on the concrete, the steel reinforcement (before patching) and the CFRP strips. Thus, a full strain profile could be drawn for the constant moment zone at each applied load level.

Fig. 3. HC-Type Girder after rehabilitation using CFRP strips bonded to the soffit of the web (left) and CFRP sheets bonded at the end of the web (right).

Without the externally bonded CFRP strips, the nominal ultimate moment of the girders was calculated to be 987 kN·m. With the bonded CFRP strips, the nominal moment was calculated based on equilibrium of forces and compatibility of strains, and estimated to be 1236 kN·m. A 25% strength enhancement was thus expected.

At a load of about 65% of the ultimate, cracks opened vertically in line with the loads, above the level of the steel reinforcement. The cracks propagated down and towards the support from the level of the steel reinforcement at an angle of about 45° until they reached the level of the CFRP strips. The cracks then propagated along the interface between the concrete and the CFRP strips (Fig. 4), occasionally passing through the concrete until the strips debonded from the girder with a thin layer of concrete

on top: a typical interfacial debonding mode of failure. The girders failed at an average ultimate moment of 998 kN·m, only an 11% strength enhancement over the experimentally recorded capacity (899 kN·m) of an unstrengthened girder (girders in their current state were also tested to yield their unstrengthened capacity in flexure and shear).

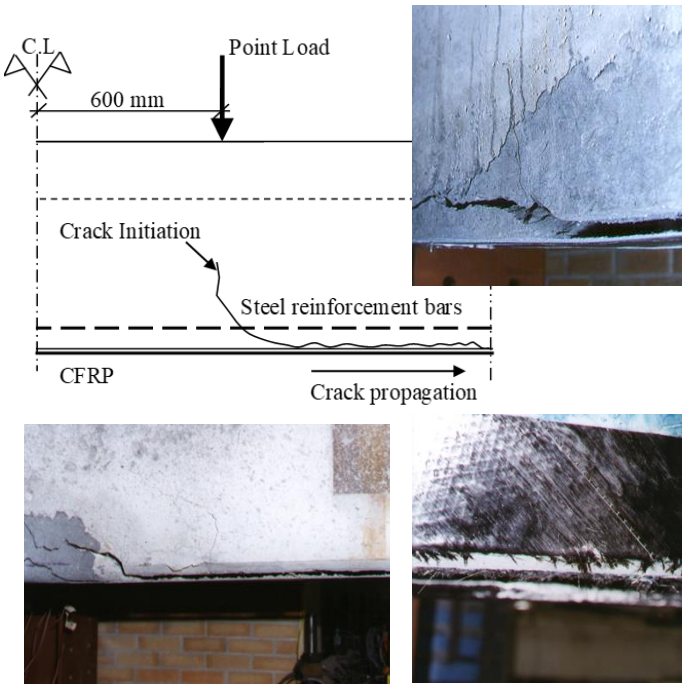

Fig. 4. Crack propagation and strip separation from the soffit of the girder (above), and CFRP strip debonding with tearing of the CFRP sheet (below).

The significant discrepancy between the ultimate moment obtained experimentally (998 kN·m) and the nominal moment estimated theoretically (1236 kN·m) can be explained using the strain profiles recorded during the test, plotted in Fig. 5.

Strain compatibility between the CFRP strips and the concrete section can be seen to occur only in the very initial stages of loading, being lost soon after crack initiation. Four different stages can be defined to generalize the behaviour of the girders retrofitted with CFRP strips. The first stage is elastic behaviour where the strain in the CFRP strips is slightly higher than the strain in the steel bars but the strains are still roughly compatible. The second stage starts with cracking of the concrete: the concrete begins to release some of its tension and the CFRP strips absorb much of this tension. Thus, the strain in the CFRP strips increases suddenly and continues to increase at a faster rate than should occur proportionally with the steel strain. In the third stage, the steel reinforcement yields: the concrete carries no tension and cracks extend to the neutral axis of the section. The strain in the steel reinforcement increases considerably with little increase in the beam capacity. Any additional tension is resisted solely by the CFRP strips. The neutral axis shifts in the beam while the strain in the CFRP-strips continues to increase, but at a slower rate compared to the steel strain. There is now a complete lack of strain compatibility.

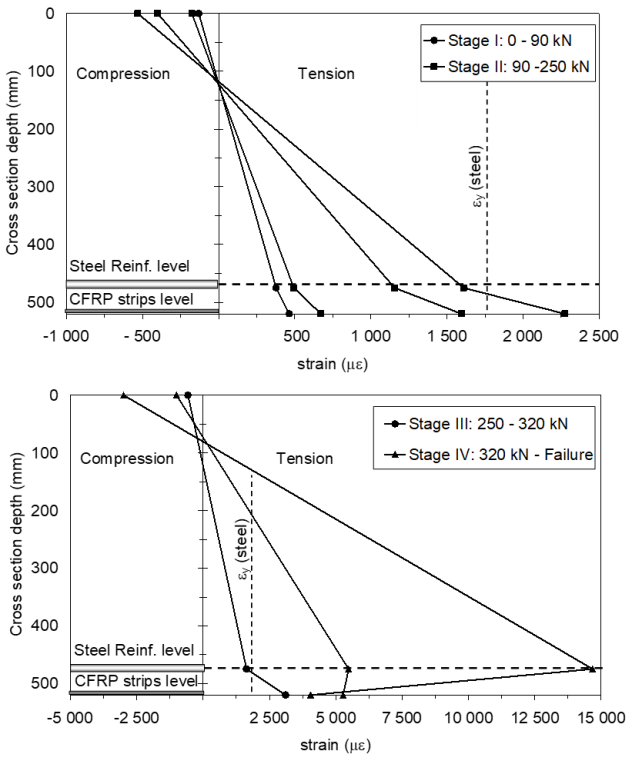

Fig. 5. Strain profile at a section within the vicinity of the constant moment zone for Girder G3 before yielding of steel reinforcement (above) and from yielding of steel reinforcement till final failure (below).

The fourth and final stage begins with the debonding of the CFRP strips. Due to the increasing forces in the strips, high shear flow occurs between the strips and the concrete. The concrete cracks because of this shear and the strips debond from the girder releasing some of their force. Strain is averaged over the unbonded length. The CFRP sheets placed at both ends of the girder for shear transfer and anchorage of the strips hold the strips, temporarily resisting debonding forces, and transferring shear to keep the CFRP strips under tension. At this stage, the CFRP strips behave as unbonded reinforcement while the strain in the steel increases dramatically. Final failure occurs when the CFRP sheets fail to hold the strips. The experimentally recorded strains show that the maximum strain reached in the CFRP strips was about 0.6% which is significantly less than the strain predicted at failure based on the assumption of strain compatibility (1.38%). Thus, debonding of the CFRP strips took place well before the assumed ultimate strain would have been reached.

2.2 *Precast Prestressed Hollow Core Slabs*

Precast-prestressed hollow core slabs are typically designed as simply supported panels. Frequently, architectural considerations require an overhanging part of the floor system to act as a cantilever. In so doing, the hollow core slabs are subject to negative moments in contrast to typical usage. To improve the negative moment resistance of the hollow core slabs, CFRP strips (S&P CFK 200/2000® 100 mm wide by 1.4 mm thick) were bonded to the top side of full-scale hollow core slabs (Fig. 6) in the negative moment zone using MBRACE adhesive HT65®.

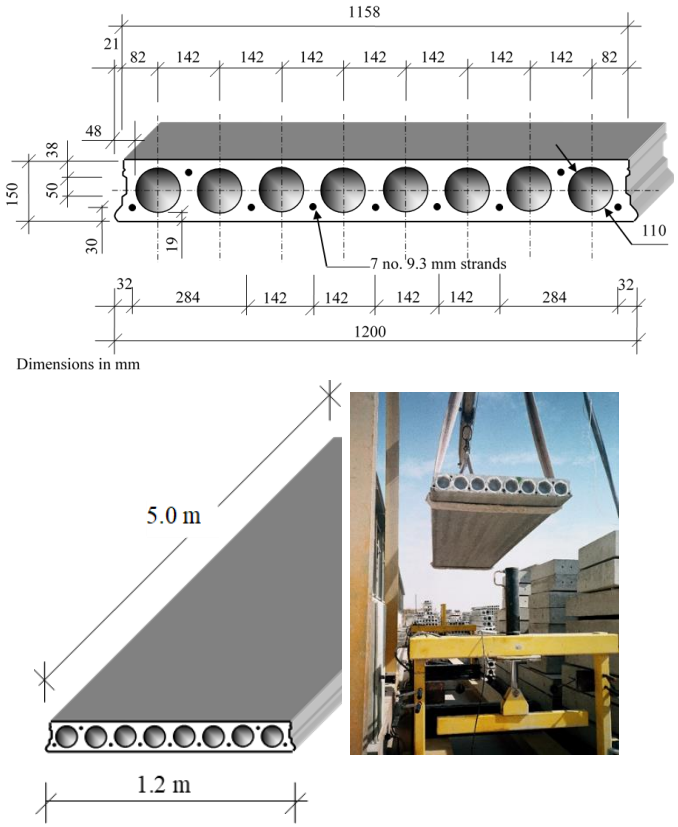

Fig. 6. Details of the precast-prestressed hollow core slabs test in the experimental programme.

The system was tested in flexure to failure. Nine slabs were tested in three series: the first series was the control, the second had only longitudinally bonded strips and the third series had transversely bonded strips at the ends of the longitudinal strips. The second series (longitudinally bonded CFRP strips) is the series considered here. Series 3 slabs were not considered herein as they present special case of broken bond between the strands and the concrete which is not the scope of the current paper.

Transverse cracks formed in the negative moment zone over the support of the overhanging cantilever on the top surface of the slab. The cracks did not immediately cross the CFRP strips after they appeared, but widened with more cracks appearing in different parts of the negative moment zone with increasing the load. In the early stages, the cracks formed between the three strips and were not aligned (Fig. 7). Failure occurred when the major flexural crack (the one over the support) extended to reach the CFRP strips then ran longitudinally along the interface between the concrete and the CFRP strips in the epoxy adhesive layer, causing debonding of the strips from the concrete surface (Fig. 7): typical intermediate flexural crack-induced interfacial debonding.

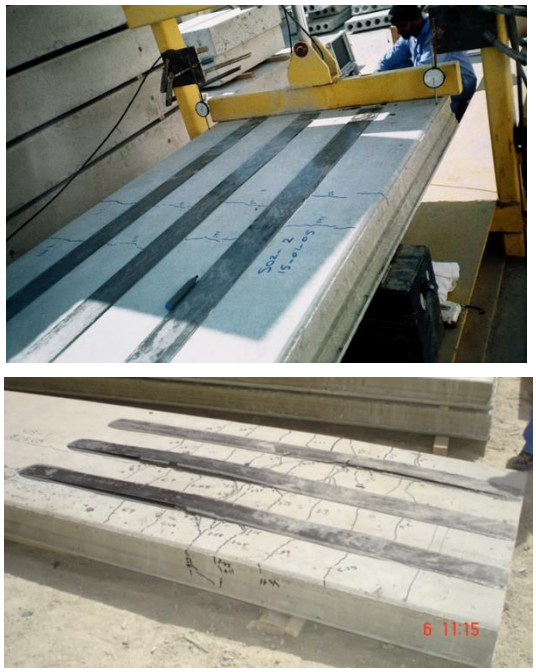

Fig. 7. Hollow core slabs with bonded FRP (above) and interfacial debonding of the strips at failure (below).

The cantilever tip displacement is plotted against the negative moment over the support in Fig. 8. Only negative moment resistance was considered since the objective of these tests was to increase the strength of HCS when the have the unusual cantilever as mentioned earlier. It is evident from Fig. 8 that bonding the CFRP strips to the precast-prestressed hollow core slabs significantly increased the negative moment resistance of the slabs. The cracking moments were increased 1.83 to 2.25 times that of the control slabs while the ultimate moments were enhanced by 2.77 to 5.74 times that of the control slabs. However, once again failure occurred prematurely due to interfacial debonding.

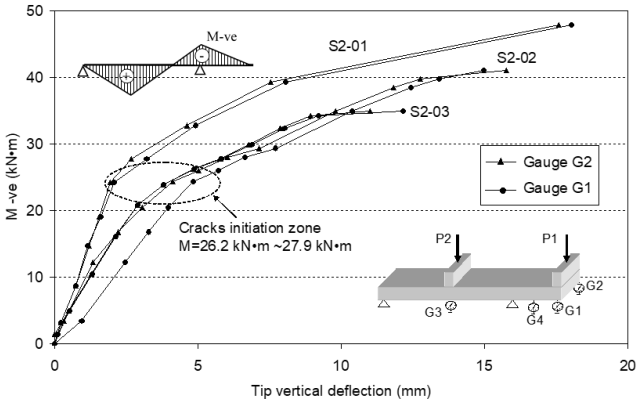

Fig. 8. Negative moment versus cantilever deflection for hollow core slabs with top-longitudinally bonded CFRP strips.

The nominal moment of the prestressed slabs with the surface-bonded CFRP strips was predicted based on the assumptions of strain compatibility and equilibrium of forces. The maximum compressive concrete strain was limited to 0.0035 and the maximum tensile CFRP strain is was limited to 0.007 (limits matching the CSA S806-02 and close to those required by the ACI 440.2-08). These procedures yield a nominal moment of 115 kN·m, which is significantly higher (2.8 times) than the experimentally recorded ultimate moment of 41.3±6.5 kN·m. It is evident from these calculations that strain compatibility is again lacking and that the flexural failure mode should not be considered alone.

When the intermediate crack-induced debonding mode was implemented in nominal moment prediction procedures via limiting the stress in the CFRP strips to the ultimate intermediate crack-induced debonding strength, the nominal moment was determined to be 67.5 kN·m, 63% higher than the average experimental ultimate moment. The remaining discrepancy indicates that the crack-induced debonding model adopted is still in need for further refinement.

2.3 *Reinforced Concrete Beam Specimens*

Twelve simply supported reinforced concrete beams with soffit bonded CFRP strips were tested monotonically in flexure in four-point loading (Fig. 9). The outcomes of these tests are summarized in Table 1. The CFRP strips were externally anchored as they covered the full length of the beam span, and were trapped between the beam and its supports.

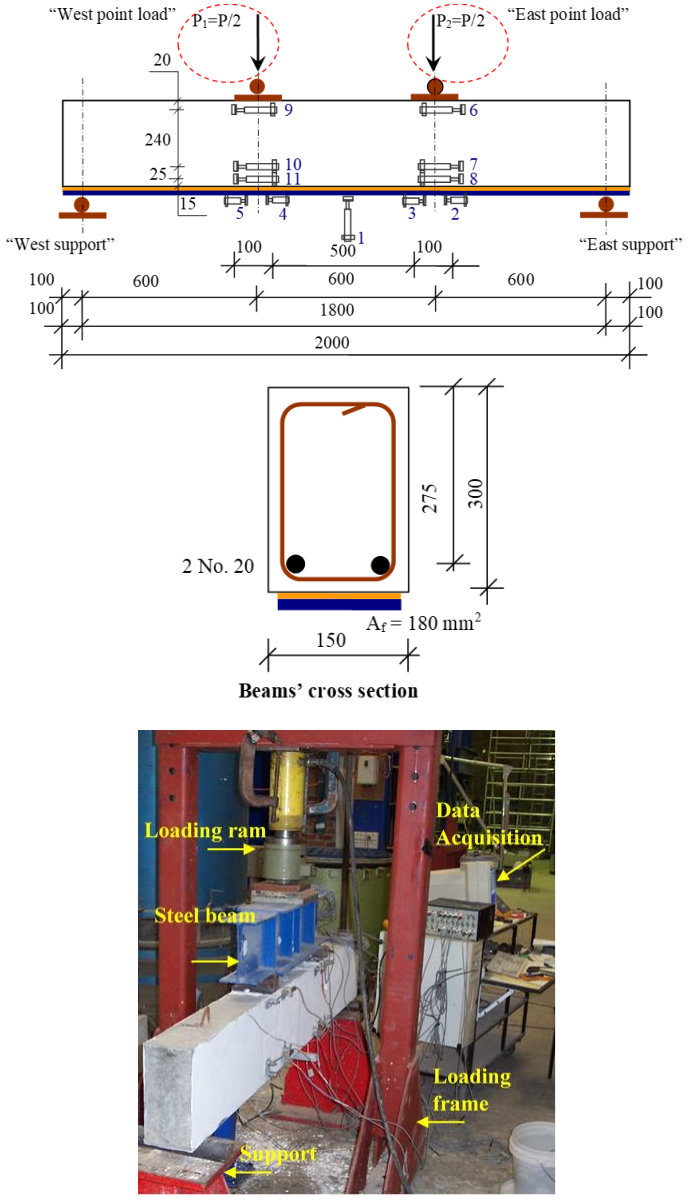

Fig. 9. Instrumentation of the tested beams and cross section of the tested beam.

For "high" or "moderate" concrete strength and "adequate" shear reinforcement beams (beams 1 to 4), flexural cracks appeared in the constant moment region with shear cracks forming within the shear span as expected. Simultaneously, the CFRP strips began to debond from the beam at one end beyond the support. The reaction force provided by the support prevented this debonding from leading to total separation of the laminate from the beams. Failures occurred when an intermediate inclined crack progressed from the level of the steel reinforcement down to the external CFRP laminate and back toward the support (Fig. 10). After failure, some concrete remained bonded to the laminate, indicating that failure progressed through the concrete cover and not through the adhesive layer. As the concrete in the constant moment region did not crush, failure thus

appeared to result from the intermediate flexure crack-induced debonding.

Typical strain distributions corresponding to 20%, 40%, 60%, 80% and 100% of the ultimate load are plotted in Fig. 11 for Beam 1. It is evident that strain compatibility between the CFRP strip and the concrete was lost in the section in line with the loading point where debonding of the strip occurred at a very early stage of loading, but the support, acting as an external anchor, held the CFRP in place.

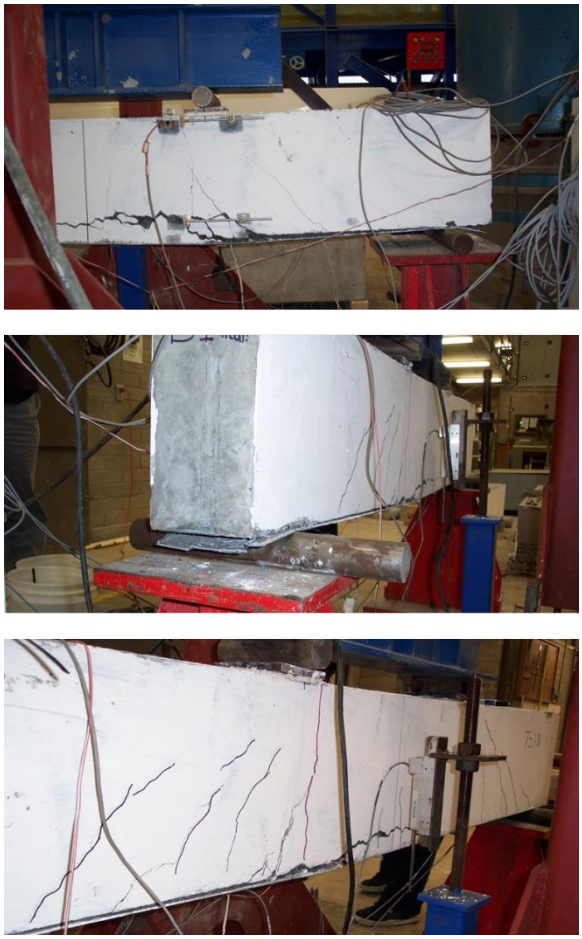

Fig. 10. Failure of Beam 1 in an intermediate flexure crack-induced debonding mode in front (above), end (middle) and back (below) views of the beam.

In the second section, under the other point load, strain compatibility was also lost between 40% and 60% of the ultimate load. This loss of strain compatibility was found in all four of these beams, in agreement with the findings and arguments of other investigations (Sayed-Ahmed 2004, Brena et al. 2003, Esfahani et al. 2007). The strain in the CFRP strips recorded at the ultimate load varied between 0.38% and 0.82% under each load point - values well beneath the ultimate breaking strain of 1.7%. This result indicates that less than half of the CFRP capacity was utilized. At ultimate load, the sharply reduced reading of the CFRP strain (0.38%) under the East point load shown in Fig. 11 is caused by the severe cracking of the concrete and debonding of the CFRP in the vicinity of the strain gauge. The other beams of this group displayed similar behaviour to this beam.

For beams 9 to 12 with "low" concrete strength and "adequate" shear reinforcement, failure occurred in two distinct modes: concrete crushing in the constant moment region and intermediate crack-induced interfacial debonding. During testing it was observed that compressive failure of the concrete occurred prior to separation of the CFRP laminate from the beam. Crushing occurred away from the external load points. Cracking resulting from the strip separation extended into the constant moment region along the line of the steel reinforcement.

The strain distributions for Beam 9 are plotted in Fig. 12, being representative of this group of beams: the lack of strain compatibility between the CFRP strips and the concrete section is again confirmed from the early stages of loading. The maximum values of the CFRP strain measured were 0.56% and 0.66% at the two sections, utilizing only 39% of the CFRP capacity.

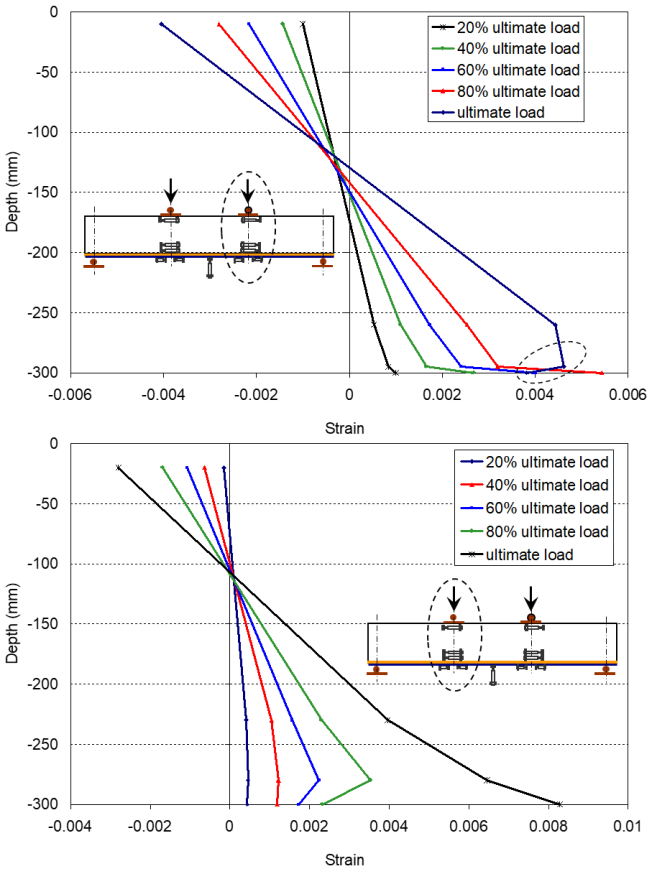

Fig. 11. Strain profiles for Beam 1 at sections under the East point load (above) and under the West point load (below).

For Beams 5 and 6 with "low" concrete strength and "high" shear reinforcement, cracking progressed similarly to the previous Beams 1 to 4 and in this instance the tendency of the laminate to peel away from

the beam beyond the support tore a chunk of concrete from the beam which remained bonded to the laminate (Fig. 13). Two distinct failures were observed for these beams. Like the previous cases, a crack propagated from the steel reinforcement level to the CFRP strips and back to the support separating the CFRP strip from the beam with some concrete remaining bonded to the strip: distinct intermediate crack-induced interfacial debonding. However, crushing of the concrete in the constant moment region was also apparent: compressive failure of the concrete was the limiting factor for this beam and the debonding occurred interactively with the concrete crushing.

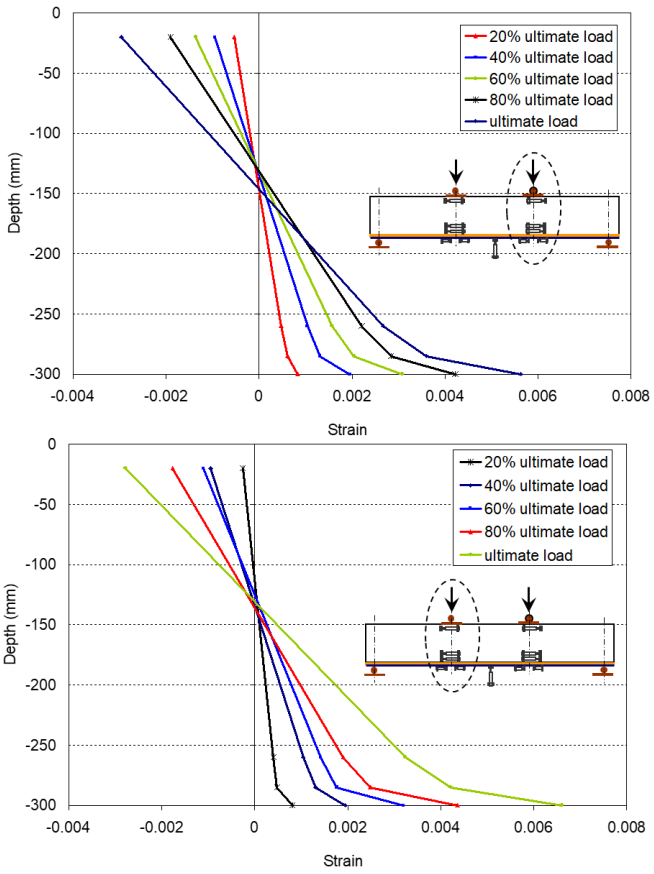

Fig 12. Strain profiles for Beam 9 at sections under the East point load (above) and under the West point load (below).

Despite the significantly reduced concrete strength compared to Beams 1 to 4, the ultimate load capacity was only marginally less than, and in some cases slightly higher than those beams. Shifting of the primary failure mode from the premature intermediate crack-induced debonding to concrete crushing (after steel yielding) has allowed more efficient use of the concrete compression region.

The strain distributions across the depth under the two point loads are plotted in Fig. 14 for Beam 5, with similar results obtained for Beam 6. Again, the figure indicates the incompatibility between the CFRP strain and the concrete strain particularly for the section in line with the West point load. However, the degree of strain incompatibility at ultimate load is less severe compared to Beams 1 to 4 where failure was solely from crack-induced interfacial debonding. The CFRP strain gauges provided strains at the ultimate load of 0.53% and 0.62% for Beam 5, and 0.52% and 0.60% for Beam 6, implying that only about a third of the CFRP capacity was utilized. Thus altering the failure mode did not increase the efficiency of use of the CFRP strip.

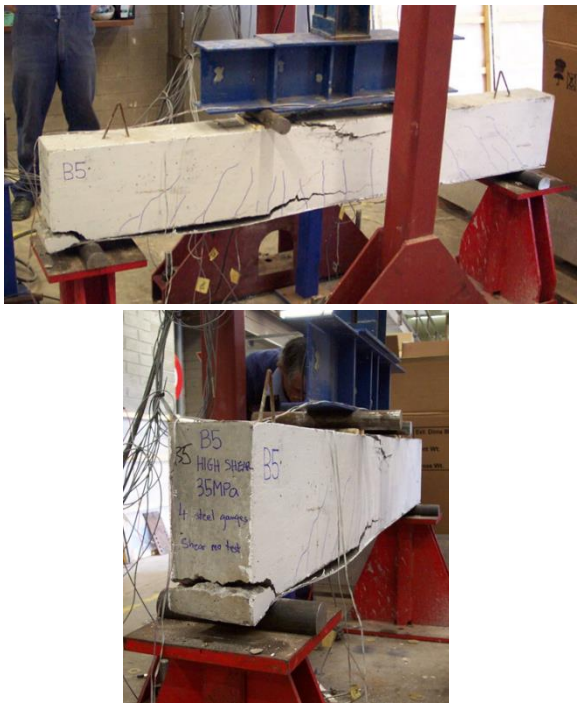

Fig. 13. Failure of Beam 5 in concrete crushing acting interactively with intermediate crack-induced debonding mode.

For Beams 7 and 8 with "low" concrete strength and "low" shear reinforcement, a distinctive mode of failure was evident (Fig. 15). Shear failure was the primary mode, but acting interactively with critical diagonal crack-induced interfacial debonding. During loading, a shear crack developed and traversed the entire depth of the beam, extending from the location of the external load point to the CFRP laminate. In Beam 7, the crack was steeper in the middle region of the beam than in the upper and lower portions, whereas for Beam 8, the slope was more uniform.

Once the crack reached the CFRP strip, propagation proceeded more slowly than in previous tests back to the support, separating the CFRP strip from the beam, again distinct crack-induced interfacial debonding. At failure, some concrete crushing occurred under a load point. This may have been a localized effect as it only occurred in the vicinity of a point load, but it also suggests the flexural and shear capacities of the beams were nearly equal.

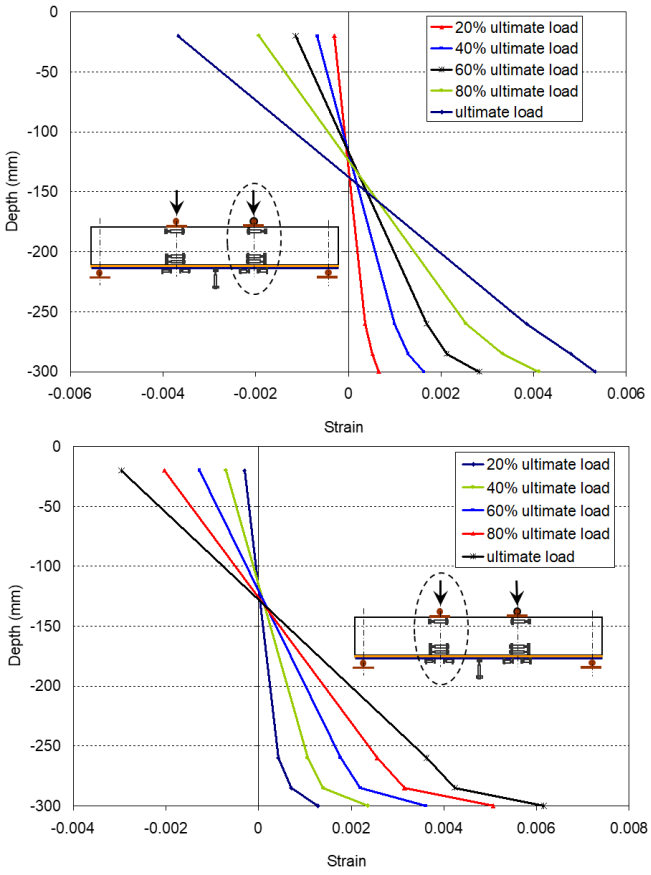

Figure 14. Strain profiles for Beam 5 at sections under the East point load (above) and under the West point load (below).

Figure 15. Failure of Beam 7 in shear acting interactively with diagonal crack-induced interfacial debonding of the CFRP.

The strain distributions in the concrete and the CFRP strip for Beam 7 in the same two sections as before are plotted in Fig. 16. There is a lack of strain compatibility between the CFRP strip and the concrete section from the very early stages of loading. The maximum CFRP strain in Beam 7 was 0.49%, implying only 29% of the CFRP capacity was used. Similarly, in Beam 8, the maximum recorded CFRP strains were 0.48 and 0.65%, using only 38% of the CFRP capacity. Thus, altering the failure mode neither increased the efficiency of CFRP usage nor changed the incompatibility of strain between the CFRP strip and the concrete section.

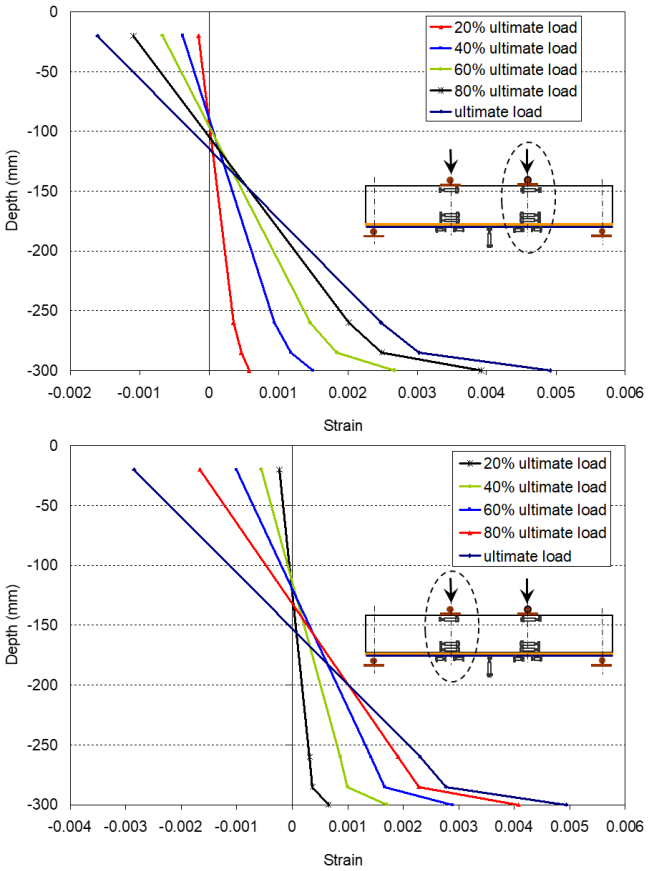

Figure 16. Strain profiles for Beam 7 at sections under the East point load (above) and under the West point load (below).

Three modes of failure were therefore observed in this testing programme: concrete crushing, shear failure and crack-induced interfacial debonding. Depending on the concrete compressive strength and the shear strength of the beam, interactive failure modes were also observed: interaction between concrete crushing and interfacial debonding, or shear failure and interfacial debonding.

It is clear from this investigation that concrete strength has a significant effect on the failure mode and hence, the ultimate load reached during the test. Generally, the ultimate load sustained by these RC beams with bonded CFRP strips was found to increase with increasing concrete compressive strength. The ultimate loads of beams under-reinforced for

shear were lower than those for beams adequately- or over-reinforced for shear.

Strain compatibility between the CFRP strips and the concrete section was lost from the early stages of loading in all twelve of these RC beams with bonded CFRP strips. Increasing the concrete compressive strength or the shear resistance of the beam had no effect on this behaviour. The strain measurements also revealed that the usage efficiency of the bonded CFRP strip was reduced because of the interfacial debonding.

3 PROPOSED PROCEDURES FOR PREDICTION OF NOMINAL MOMENT

The ACI 440.2R-08 and CSA S806-02 specifications may be adopted to predict the nominal moments of reinforced concrete members strengthened in flexure using externally bonded CFRP laminates. Both specifications base the nominal moment on strain compatibility, equilibrium of forces and controlling the mode of failure provided that: a) plane sections remain plane, b) perfect bond exists between the FRP strips and the concrete, c) the maximum compressive concrete strain is 0.003 (ACI 440.2R-08) or 0.0035 (CSA S806-02), and d) the maximum FRP tensile strain is:

$$\text{CSA S806}-02:\quad \varepsilon_{fd} = 0.007 \tag{1}$$

$$\text{ACI 440.2R}-0.8:\quad \varepsilon_{fd} = 0.41\sqrt{f_c' / (nE_f t_f)} \le 0.9\varepsilon_{fu} = 0.9\left(C_E \varepsilon_{fu}^*\right)$$

where E_f is tensile modulus of elasticity of FRP, C_E is an environmental reduction factor, n is the number of plies of the FRP laminates, t_f is the laminates thickness, f_c' is the 28 days concrete cylinder compressive strength, ε_{fu}^* and is the ultimate rupture strain of the FRP laminates. The above limit on the FRP strain is defined in order to prevent intermediate crack-induced debonding failure (Teng et al. 2001, 2002 and 2004). However, it is proposed to replace the strain limit with a limit on the FRP stress corresponding to the debonding strength using an approach similar to the one adopted by Teng et al. (2002, 2004) with minor modifications to the debonding strength equation.

Referring to Fig. 17, equilibrium of forces yields

$$C = T \quad \rightarrow \alpha_1 f_c'(\beta_1 c)(b) = A_{sc}F_{sc} + A_s F_s + A_f F_f \tag{2}$$

where f_c' is the concrete compressive strength, b is the slab width, A_s and A_{sc} are the areas of the tension and compression steel reinforcements, respectively, F_s and F_{sc} are the stresses in the tension and compression steel reinforcing, respectively, A_f is the area of the FRP laminates and F_f the stress in the FRP laminates, and α_1 and β_1 are coefficients for the equivalent concrete compression block defined by the codes of practice.

Compatibility of strains requires that

$$\varepsilon_s = \varepsilon_{cu}\frac{d_s - c}{c};\quad \varepsilon_{sc} = \varepsilon_{cu}\frac{d_s' - c}{c};\quad \varepsilon_f = \varepsilon_{cu}\frac{t - c}{c} \tag{3}$$

where ε_{cu} is the maximum compressive (crushing) strain of concrete, ε_s and ε_{sc} are the strains in the tension and compression top prestressing strands respectively, ε_f is the strain in the CFRP strips, t is the member height, d_s and d_s' are the depths to the tension and compression reinforcements, respectively, and c is the depth of the compression part of the cross section.

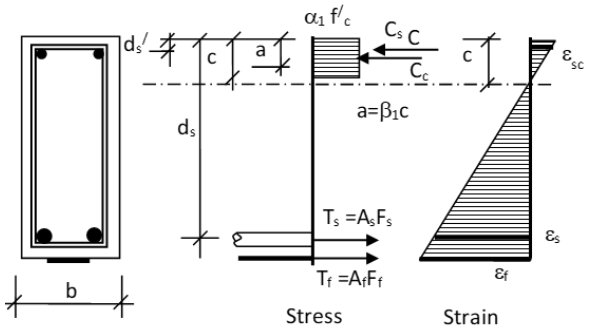

Fig. 17. Stress and strain distribution at ultimate load along the cross section of the CFRP strengthened RC beams assuming full strain compatibility.

The stresses in the bottom and top steel reinforcement and in the FRP laminates are given by

$$F_s = E_s \cdot \varepsilon_s \le F_y \qquad F_{sc} = E_s \cdot \varepsilon_{sc} \le F_y$$
$$F_f = E_f \cdot \varepsilon_f \le F_{fu} = C_E F_{fu}^* \tag{4}$$

where n is the number of plies of the FRP laminates, t_f is the laminates thickness, α_{db} is a coefficient which was calibrated against test data of beams and slabs[1,8] (found to be 0.4) and β_b and β_l are width and bond length coefficients, respectively, determined by

$$\beta_p = \sqrt{(2 - b_f / b)/(1 + b_f / b)} \tag{5a}$$

$$\begin{aligned} L \geq L_e = \sqrt{E_f t_f / \sqrt{f_c'}} \qquad & \beta_L = 1.0 \\ L < L_e = \sqrt{E_f t_f / \sqrt{f_c'}} \qquad & \beta_L = \sin\left[\pi L / 2L_e\right] \end{aligned} \tag{5b}$$

where L_e is the effective bond length, L is the length of the FRP laminates E_f is the elastic modulus of the FRP laminates, t_f is the thickness of the laminates, b_f is the width of the FRP laminates and b is the cross section's width. It is worth mentioning that the above limit on FRP laminate stress yields the same value as the limit defined in the ACI 440.2R-08 when the length of the bonded laminates is greater than the effective length ($\beta_L=1$) and the laminates cover half the width of the concrete section ($\beta_p=1$).

The stress in the FRP laminates is then obtained using the following equation which should replace the second part of Equation 4:

$$F_f = minimum\ of: \begin{vmatrix} E_f \varepsilon_f \\ F_{db} \\ F_{fu} = C_E F_{fu}^* \end{vmatrix} \tag{6}$$

The nominal moment M_n of the strengthened section is given by

$$\begin{aligned} M_n = A_f F_f (t - \frac{(\beta_1 c)}{2}) + \\ A_s F_s (d_s - \frac{(\beta_1 c)}{2}) + A_{sc} F_{sc} (\frac{(\beta_1 c)}{2} - d_s') \end{aligned} \tag{7}$$

Applying these procedures to the beam specimens (Table 1) reveals a good estimate for the nominal moments of all beams except those that failed in shear or interactive failure between shear and interfacial debonding. Further work is needed in respect of this latter failure mode.

Table 1. Results of the experimental investigation of the twelve beam specimens.

Beam	f_c' (MPa)	Stirrups Spacing (mm)	Failure load (kN)	Failure Moment (kN·m)	Predicted Moment (kN·m)	Failure mode	FRP strain (%)	
							West load	East load
1	69.9±2.3	160	449	134.7	127.8	IC	0.83	0.38
4	64.1±2.2	160	426	127.8	122.9	IC	0.43	0.59
2	65.1±0.7	160	433	129.9	123.7	IC	0.62	0.54
3	57.2±2.0	160	408	122.4	116.7	IC	0.47	0.59
9	46.1±1.9	160	406	121.8	109	CC+IC	0.66	0.56
10	48.8±2.0	160	389	116.7	111	CC+IC	0.58	0.56
11	41.6±0.4	160	395	118.5	105.1	CC+IC	0.59	0.57
12	40.3±1.3	160	371	111.3	103.9	CC+IC	0.57	0.49
5	45.4±2.9	100	425	127.5	108.4	CC+IC	0.62	0.53
6	43.7±1.5	100	410	123	107	CC+IC	0.59	0.52
7	43.7±3.5	320	343	102.9	107	SF+CDC	0.49	0.49
8	41.8±0.4	320	347	104.1	105.3	SF+CDC	0.48	0.65

*IC= intermediate flexure or flexure shear crack-induced debonding, CC = concrete crushing, SF = shear failure, and CDC= critical diagonal crack-induced debonding.

4 CONCLUSIONS

Bonding FRP laminates to the tension side of reinforced concrete members subject to flexure can enhance the flexural capacity of such members significantly. A better understanding of the causes of failure for these FRP strengthened members will allow for more precise designs that will balance safety and cost. The experimental investigations performed on slabs and beams with externally bonded FRP laminates revealed clearly that crack induced debonding failure is one of the major factors affecting the flexural strength of the member and should be explicitly considered in calculating the nominal moment.

A recently proposed debonding model was slightly revised and adopted together with code provisions in estimating the nominal moments. The model showed reasonable agreement with the test results. Furthermore, the tests proved that strain compatibility between the FRP laminates and the concrete section is always lost from the early stages of loading. The strain measurements also revealed that the usage efficiency of the bonded CFRP strip was reduced because of the interfacial debonding. A model is proposed following the procedures in the same codes but including the debonding strength in the calculation of

the flexural strength of reinforced concrete members with externally bonded FRP laminates.

REFERENCES

1. ACI 440.2R-08. Guide for the Design and Construction of Externally Bonded FRP Systems for Strengthening Concrete Structures. Reported by ACI Committee 440. American Concrete Institute, USA. 2008.
2. Bakay R., Sayed-Ahmed E.Y., and Shrive N.G. Interfacial Debonding Failure for Reinforced Concrete Beams Strengthened with CFRP Strips, Canadian Journal of Civil Engineering, 2009, 36, No. 1: pp. 103-121.
3. BREÑA S.F., BRAMBLETT R.M., WOOD S.L., and KREGER M.E. Increasing flexural capacity of reinforced concrete beams using carbon fibre reinforced polymer composites. ACI Structural Journal, 2003, 100, No. 1, 36-46.
4. Chen J.F., and Teng J.G. Anchorage strength model for FRP and steel plates attached to concrete. Journal of Structural Engineering, ASCE, 2001, 127, No. 7, 784-791.
5. Choi E, Utui N, Kim HS. Experimental and analytical investigations on debonding of hybrid FRPs for flexural strengthening of RC beams. Composites Part B: Engineering. 2013, 45, No. 1, 248-56.
6. CSA S806-02. Design and Construction of Building Components with Fibre-Reinforced Polymers. Canadian Standards Association CSA, Ontario, Canada. 2002.
7. D'Antino T, Pellegrino C, Carloni C, Sneed LH, Giacomin G. Experimental analysis of the bond behavior of glass, carbon, and steel FRCM composites. InKey Engineering Materials 2015 (Vol. 624, pp. 371-378). Trans Tech Publications.
8. Esfahani M.R., Kianoush M.R., and Tajari A.R. Flexural behaviour of reinforced concrete beams strengthened by CFRP sheets. Engineering Structures, Elsevier. 2007
9. Hensher DA. Fiber-reinforced-plastic (FRP) reinforcement for concrete structures: properties and applications. Elsevier; 2016 Jan 22.
10. Hosny A., Abdelrahamn A.A., Sayed-Ahmed E.Y., and Alhlaby, N.A. CFRP Strengthening of Prestressed/Precast Hollow Core Slabs to Resist Negative Moments. Proceedings, 10th Arab Structural Engineering Conference (10ASEC), Kuwait, Nov. 2006.
11. Hosny A.A., Sayed-Ahmed E.Y., Abdelrahamn A.A., and Alhlaby, N.A. Strengthening precast-prestressed hollow core slabs to resist negative moments using CFRP strips: an experimental investigation and a critical review of CSA 806-02. Canadian Journal of Civil Engineering, 2006, 33, No. 8, 955-967.
12. Hosseini A, Mostofinejad D. Effective bond length of FRP-to-concrete adhesively-bonded joints: Experimental evaluation of existing models. International Journal of Adhesion and Adhesives. 2014, 48, 150-8.
13. Lee Y. J., Boothby T. E., and Bakis, C. E. Slip modulus of FRP sheets bonded to concrete. Journal of Composites for Construction, 1999, 3, No. 4, 161-167.
14. Lu X.Z., Teng J.G., Ye L.P., and Jiang J.J. Bond-slip models for FRP sheets/plates bonded to concrete. Engineering Structures, Elsevier, 2005, 27, No. 6, 920-937.
15. Meier U. Strengthening of structures using carbon fibre/epoxy composites, Construction and Building Materials, 1995, 9, No. 6, 341-351.
16. Oehlers D.J., Park S.M., and Mohamed Ali M.S. A structural engineering approach to adhesive bonding longitudinal plates to RC beams and slabs. Composite: Part A, 2003, 34, No. 12, 887-897.
17. Ombres L. Prediction of intermediate crack debonding failure in FRP-strengthened reinforced concrete beams. Composite Structures. 2010; 92, No. 2, 322-329.
18. Ombres L. Debonding analysis of reinforced concrete beams strengthened with fibre reinforced cementitious mortar. Engineering Fracture Mechanics. 2012, 81, 94-109.
19. Sayed-Ahmed, E.Y., Bakay, R., and Shrive, N.G. 2009. Bond Strength of FRP Laminates to Concrete: State-of-the-Art Review. Electronic Journal of Structural Engineering. 9: 45-61, Sept 2009.
20. Sayed-Ahmed E.Y., Riad A.H., and Shrive N.G. Flexural strengthening of precast reinforced concrete bridge girders using bonded CFRP strips or external post-tensioning. Canadian Journal of Civil Engineering, 2004, 31, No. 3, 499-512.
21. Smith S.T., and Teng J.G. FRP strengthened RC beams – I: Review of debonding strength models. Engineering Structures, Elsevier, 2002, 24, No. 4, 385-395.
22. Smith S.T., and Teng J.G. FRP strengthened RC beams – II: assessment of debonding strength models. Engineering Structures, 2002, 24, No. 4, 397-417.
23. Spadea G., Bencardino F., and Swamy R. N. Structural behavior of composite RC beams with externally bonded CFRP. Journal of Composites for Construction, ASCE, 1998, 2, No. 3, 132-137.
24. Teng J.G., Chen J.F., Smith S.T., and Lam L. FRP strengthened RC structures. Academic Press Ltd, Wiley, West Sussex, UK, 266 pp., 2002.
25. Teng J.G., Lu X.Z., Ye. L.P., and Jiang J.J. Recent research on intermediate crack induced debonding in FRP-strengthened RC beams. Proceedings of the 4th International Conference on Advanced Composite Materials in Bridges and Structures, Calgary, Canada, 20-23 July, 2004, CSCE. CD-proceedings.
26. Teng J. G., Smith S. T., Yao J., and Hen J. F. Intermediate Crack Induced Debonding in RC Beams and Slabs, Construction and Building Materials, 2001, 17, No. 6, 447-462.
27. Triantafillou T. C., and Plevris N. Strengthening of RC beams with epoxy-bonded fibre-composite materials. Materials and Structures, RILEM, 1992, 25, No. 148, 201-211.
28. Uedat., Dai J.G., and Sato Y. A nonlinear bond stress-slip relationship for FRP sheet-concrete interface. Proceedings of international symposium on latest achievement of technology and research on retrofitting concrete structures, Kyoto, Japan, July 14-15, 2003, pp. 113-120.
29. Yuan H., Teng J.G., Seracino R., Wu Z.S., and Yao J. Full-range behabiour of FRP-to-concrete bonded joints. Engineering Structures, Elsevier, 2004, 26, No.5, 553-564.
30. Zhu J.T., Wang X.L., Kang X.D., Li K. Analysis of interfacial bonding characteristics of CFRP-concrete under fatigue loading. Construction and Building Materials. 2016, 126, 823-33.
31. Zhou Y, Gou M, Zhang F, Zhang S, Wang D. Reinforced concrete beams strengthened with carbon fiber reinforced polymer by friction hybrid bond technique: Experimental investigation. Materials & Design. 2013, 50, 130-9.